

# A definition of hydraulic efficiency of the soil-plant-atmosphere continuum based on electric circuit theory

GEORGIOS XENAKIS<sup>1\*</sup>

<sup>1</sup>Forest Research, Northern Research Station, Roslin, Midlothian, EH25 9SY, UK

<sup>6</sup>\*Corresponding author. E-mail: georgios.xenakis@forestresearch.gov.uk Telephone: 0044 300 067 5999

7 Abstract

## 8 Keywords:

9.1 Introduction

The climate is changing, and intra-annual and inter-annual precipitation patterns are shifting (Zhou et al., 2019). Plants respond to environmental changes because of their physiological plasticity (Kramp et al., 2022). However, evolutionary responses to changes in the climate take hundreds of years. Climate change has accelerated shifts to precipitation giving limited time for vegetation (and trees in this case) to adapt. These shifts result in severe water stress for species not already adapted to limited water resources, leading to the catastrophic collapse of the tree water transport system (Arend et al., 2021) and, ultimately, canopy dieback (Losso et al., 2022) or mortality (McDowell et al., 2008; Rowland et al., 2015; Choat et al., 2018). Therefore, any future human intervention to enhance forest resilience and preserve future forest resources requires a quick and reliable method for quantifying water stress.

Traditionally we can assess water stress levels using gas exchange ([Rehschuh et al., 2020](#)), leaf turgor loss ([Zhu et al., 2018](#)) or plant hydraulic traits such as safety and efficiency ([Charra-](#)

22 Vaskou et al., 2012; Zhang et al., 2013; van der Sande et al., 2019; Schumann et al., 2019;  
23 Fuchs et al., 2021). These approaches offer reliable measurements at the plant level, giving us  
24 valuable insights into water regulation mechanisms and limitations of individual species. However,  
25 because of their mostly lab-based nature, they offer data for a limited range of environmental and  
26 growing conditions insufficient to explore interactions of the soil-plant-atmosphere (SPA) during  
27 water-limited periods.

28 In a global assessment of the variability of hydraulic safety, Choat et al. (2012) showed that  
29 it was not dependent on precipitation, with drought stress appearing in both wet and dry for-  
30 est ecosystems. Vapour pressure deficit ( $D$ ) is the main driver for water uptake and movement  
31 (Grossiord et al., 2020) and hence one of the factors directly affecting water stress levels. How-  
32 ever, Carminati and Javaux (2020) also argued that soil water potential had a greater contribution  
33 in driving stomatal closure. So overall, for a more responsive way of accessing water stress, we  
34 must look at the SPA holistically and consider these three essential elements: 1) quantify the re-  
35 sistance of the plant and assess how it changes over time as water stress continuous, 2) quantify  
36 the available soil water available for plant uptake and 3) quantify the force the atmosphere applies  
37 on the soil-plant continuum and how it affects the levels of waters stress plants are experienc-  
38 ing. Therefore, we must develop a method for quantifying water stress based on fundamental  
39 principles of water transport through the SPA continuum that amalgamates these three important  
40 elements in a continuous, real-time, simple, cost-effective, and robust way. Continuous because  
41 it will allow us to capture temporal water stress variability under a broader range of environmental  
42 conditions focused on in-situ application. Simple because the method must be based on easily  
43 measurable variables. Finally, cost-effective because the method must apply to modern technolo-  
44 gies quantifying water stress in a near real-time way offering spatial replication and multi-scale  
45 application.

46 There are multiple approaches for monitoring water stress from the tree to the regional level  
47 and with different temporal scales. For example, sap flow-based measurements at the tree level  
48 are based on monitoring water flow through the xylem and identifying and quantifying water stress  
49 by combining measurements with other traits, such as leaf water potential (Nadezhina, 1999),  
50 through fitted models with soil water availability (Granier et al., 2000), or water stress indices  
51 based on transpiration (Venturin et al., 2020), and climatic and soil drought (Naithani et al., 2012).

52 Interestingly, the approach by Naithani et al. (2012) has encapsulated the three elements I men-  
53 tioned before for a relevant water stress indicator of the SPA. However, despite the scientifically  
54 sound basis, it is a method that requires considerable post-data-collection processing to identify  
55 water limitations. On the other hand, Nackley et al. (2020) offer a sap flow-based water stress  
56 index considering each of my fundamental elements but with also considerable additional compu-  
57 tational requirements.

58 Water stress can also be quantified through temperature-based methods (Drechsler et al.,  
59 2019), some of which use thermal cameras (Reinert et al., 2012) to look at canopy temperature.  
60 In contrast, others have used evapotranspiration (Han et al., 2018; Carminati and Javaux, 2020)  
61 or even a two-source energy balance model (Nieto et al., 2022) to derive stress indices. Other  
62 methods focus on monitoring stem shrinkage caused by changes in its water content (Zweifel  
63 et al., 2005; Conejero et al., 2007; Alizadeh et al., 2021; Knüsel et al., 2021), statistical models  
64 between soil water potential with climatic drought indices (Vido et al., 2016), leaf water potential  
65 with soil water and potential evapotranspiration (Nel and Berliner, 1990), or even looking at tree  
66 sway as a proxy of water stress (Ciruzzi and Loheide, 2019). More recently, Bourbia and Brodribb  
67 (2023) developed a technique for near real-time monitoring of transpiration in-situ using stem  
68 water potential inferred from optical dendrometers. Although the method provided an accurate  
69 prediction of transpiration, its fundamental principle is based on the assumption that conductance  
70 between root and stem remains constant at a diurnal scale and does not assess the soil water  
71 status. Remote sensing is also very commonly used as a method to quantify water stress at  
72 larger scales either through relationships between the photochemical reflectance index and sap  
73 flow velocities (Yang et al., 2020), normalised differences vegetation index and evapotranspiration  
74 (Feiziasl et al., 2022), direct assessment of vegetation and soil moisture through radar (Konings  
75 et al., 2021) or modelling driven by remote sensing data (Tadesse et al., 2020). This wide range  
76 of approaches to quantifying water stress makes it hard to have a method that addresses each of  
77 the three fundamental elements I proposed above.

78 Electrical engineering can offer suitable analogies to fulfil all three elements successfully. Al-  
79 though many models already have adopted electric circuits to represent water movement through  
80 the soil-plant continuum (Landsberg et al., 1976; Milne et al., 1983; Hunt et al., 1991; Williams  
81 et al., 2001; Zhuang et al., 2014), their detailed approach is best used for understanding mech-

82 anisms and feedbacks without necessarily focusing on quantifying timing, duration and intensity  
83 of water stress. So, we must look further into some fundamental electrical engineering princi-  
84 ples, also known as Electric Circuit Theory (ECT). Analogies of ECT have been used in other  
85 aspects of science, such as connectivity and conservation (McRae et al., 2008; Dickson et al.,  
86 2018), plant and animal genetics (McRae and Beier, 2007) and biochemistry (Tang et al., 2021).  
87 However, the potential of ECT has never been explored in plant ecophysiology and, particularly,  
88 water movement.

## 89 **1.1 The proposed concept**

90 I propose to adopt and adapt Electric Circuit Theory to determine the hydraulic efficiency of the  
91 SPA continuum. The novelty of this approach is the use of a single index to identify the point  
92 at which transpiration losses balance with the soil water supply. Knowing when water transport  
93 is balanced allows us to measure how long plants spend under water stress. Furthermore, we  
94 can use hydraulic efficiency to compare water usage between species, ultimately leading to an in-  
95 formed decision of species choice for planting under future climate. However, we must not confuse  
96 hydraulic efficiency with water use efficiency since the former focuses entirely on water transport,  
97 looking at the SPA as a whole. In contrast, the latter includes the element of photosynthetic ca-  
98 pacity.

### 99 **1.1.1 Definition of SPA hydraulic efficiency based on ECT**

100 To better understand how ECT applies to the SPA continuum, first, we must present some defini-  
101 tions of electrical theory and how they relate to soil-plant hydraulics. Table 1 shows five concepts:  
102 quantity, quantity flux, flux density, potential and capacitance. When describing plant hydraulics,  
103 we see the electrical potential as the difference in water potential, the electrical current as the wa-  
104 ter volume flow rate between a water potential gradient and the capacitance as the water stored  
105 for every unit of water potential gradience.

106 Here, I will use two concepts from Electric Circuit Theory. Electric power and efficiency. Electric  
107 power is defined as energy consumption divided by the time of consumption or, in other words,  
108 the force required to move electrons across a voltage gradience per unit of time. Equivalently, I  
109 propose to define the hydraulic power of the SPA as the energy consumption for moving water

110 across a water potential gradience per unit of time.

111 On the other hand, the efficiency of an electric circuit or device is defined as the device's power  
112 output divided by the total power consumption or simply the proportion of energy dissipated by the  
113 circuit that is dissipated by the load. Therefore, I propose similarly that hydraulic efficiency is  
114 defined as the power of the plant divided by the total power of the SPA continuum or simply the  
115 ratio of energy for water movement to the total energy in the SPA continuum.

### 116 1.1.2 The electric close circuit analogy

117 In my proposed analogy of the SPA, I represent the water movement at a tree scale with a simple  
118 electric circuit of two resistors and one source (Figure 1). The main reason for this oversimplifi-  
119 cation is the desire to have continuous and reliable measurements of these three elements of the  
120 circuit, which will allow an estimation of water stress.

121 Since atmospheric vapour pressure deficit controls stomatal conductance and hence the up-  
122 ward movement of water, I consider atmospheric water potential rather than leaf water potential  
123 as the "negative" term of the potential difference (Figure 1). The advantage is that we can calcu-  
124 late atmospheric water potential continuously from measurements of air temperature and relative  
125 humidity with meteorological stations placed above the tree canopy.

126 Similarly, I consider soil water potential as the "positive" term of the potential difference, creat-  
127 ing this way a source of water or a "battery" (Figure 1). We may also consider precipitation as a  
128 recharging event of this source. Continuous soil water potential measurements can be available  
129 either directly from soil tensiometers or calculated from volumetric water content data obtained  
130 with TDR sensors with generalised soil-water characteristics equations (Saxton et al., 1986).

131 The two resistors of this simplified electric circuit analogy are the soil and plant. Here, I assume  
132 that tree stem resistance is sufficient to represent whole-plant resistance (Landsberg et al., 1976;  
133 Jones, 1992; Zhuang et al., 2014). Generalised soil-water characteristic equations also estimate  
134 soil conductivity from soil texture and continuous volumetric water content data. In addition, the  
135 well-established methods of tree sap flow measurements can provide the necessary continuous  
136 measurement of tree stem resistance.

137 Although the close circuit analogy illustrated in Figure 1 is based on tree-level hydraulics, a  
138 similar analogy can be made at an ecosystem level. We can calculate water efficiency at the

139 ecosystem level using eddy covariance flux towers and measurements of evapotranspiration.

### 140 1.1.3 Calculation of hydraulic efficiency

141 Using Ohm's law, we calculate the flow of water like the current of an electric circuit as the ratio  
142 of the difference in water potential between soil and the atmosphere to the sum of soil and plant  
143 resistance (Equation 1).

$$Q = \frac{\Delta\Psi_{soil-air}}{R_{soil} + R_{plant}} \quad (1)$$

144 According to the voltage divider rule, which states that the voltage of any resistor in a serial  
145 connection is equal to the ratio of the voltage of the resistor divided by the resistance of the circuit,  
146 we can calculate the difference in water potential of the soil-plant-atmosphere using Equation 2.

$$\Delta\Psi_{SPA} = \Delta\Psi_{soil-air} \frac{R_{plant}}{R_{soil} + R_{plant}} \quad (2)$$

147 Since the power of a load resistor in an electric circuit is the product of voltage and current,  
148 similarly, we calculate the power of the SPA continuum as the product of  $\Delta\Psi_{SPA}$  and the water  
149 flow  $Q$  (Equation 3).

$$P_{SPA} = \Delta\Psi_{SPA} Q = \frac{R_{plant}\Delta\Psi_{soil-air}^2}{(R_{soil} + R_{plant})^2} \quad (3)$$

150 Substituting  $\Delta\Psi_{SPA}$  in Equation 3 with Equation 2, we determine the SPA power using its  
151 resistance and the water potential difference between soil and air. Replacing  $R_{plant}$  with  $R_{stem}$   
152 and rearranging to remove  $R_{stem}$  from the numerator, the power of the plant is given by Equation  
153 4.

$$P_{plant} = \frac{\Delta\Psi_{soil-air}^2}{R_{soil} \left( \frac{\sqrt{R_{soil}}}{\sqrt{R_{stem}}} + \frac{\sqrt{R_{stem}}}{\sqrt{R_{soil}}} \right)^2} \quad (4)$$

154 Similarly, we calculate soil power with Equation 5.

$$P_{soil} = \frac{\Delta\Psi_{soil-air}^2}{R_{stem} \left( \frac{\sqrt{R_{soil}}}{\sqrt{R_{stem}}} + \frac{\sqrt{R_{stem}}}{\sqrt{R_{soil}}} \right)^2} \quad (5)$$

155 Finally, we calculate the hydraulic efficiency as the ratio of the plant's power to the sum of soil  
156 and plant power (Equation 6).

$$\eta = \frac{P_{plant}}{P_{plant} + P_{soil}} \quad (6)$$

## 157 1.2 Objectives and aim of the study

158 In this study, based on the new proposed definition of hydraulic efficiency, I will first provide a  
159 theoretical framework for determining when trees are most efficient at water uptake and when  
160 they are likely to experience water stress. Then, using field measurements at the tree level, I will  
161 apply the theoretical framework to investigate how long they spend under water stress conditions.  
162 Furthermore, using eddy covariance data, I will apply the same principles at the ecosystem level  
163 and focus on the recent drought year of 2018. Finally, using a global database of sap flow mea-  
164 surements, I will investigate the hydraulic efficiency of several species across biomes and discuss  
165 what it means for their water use under a future water-limited climate.

166 The overall aim is to demonstrate the practical application of Electric Circuit Theory and  
167 develop a methodology for quantifying the efficiency of water transport through the soil-plant-  
168 atmosphere at different scales. Furthermore, this study aims to provide the means for quantifying  
169 the period length under water stress. In addition, I will discuss the application of this new method-  
170 ology for real-time water balance monitoring.

## 171 2 Material and methods

172 The broad focus of this study requires a range of data, from tree to ecosystem and the globe.  
173 Therefore, I used data from recently established field measurements, long-term ecosystem and  
174 meteorological data from an intensively monitored flux site and a global sap flow measurements  
175 database. All data manipulation, calculations, analyses and graphics were performed using the R  
176 software ([R Core Team, 2022](#)) and its associate packages.

177 **2.1 Study site**

178 The Harwood Forest flux monitoring site is a commercial upland conifer plantation in Northumber-  
179 land, North-East England. The site is a 40 ha second rotation, even-aged, mature Sitka spruce  
180 (*Picea sitchensis* (Bong.) Carr.), planted in 1973 on peaty-gley (cambic stagnohumic gley, WRB,  
181 FAO) soils. The top height of the stand is 26 m, with a mean tree density of 1348 trees ha<sup>-1</sup> and a  
182 leaf area index of 5.7. The site's elevation is 290 m with a slope of 2°. In 2014, a 32 m scaffolding  
183 tower was installed to monitor the carbon, energy and water fluxes with eddy covariance. For more  
184 information about the site, [Xenakis et al. \(2021\)](#).

185 **2.2 Data sources**

186 **2.2.1 Sap flow**

187 In May 2021, I installed ten SFM1 sensors (Figure 2, ICT International Ltd., Australia) and mea-  
188 sured sap flow using the heat pulse method ([Burgess et al., 2001](#)). Before installation, I conducted  
189 a diameter survey to capture any variability and sapwood area across the stand. I used a stratified  
190 sampling from a pre-existing sampling of the leaf area index. Seven transects were set up from  
191 North to South, each perpendicular to the tower in a westerly direction. Each transect had 13 plots  
192 of 5 m radius, 10 meters apart along the transect. For the diameter survey, I used the two nearest  
193 to the tower transects and measured all the trees in each plot. I split the data into five diameter  
194 classes between 7 and 57 cm and calculated the median for each class. I installed two sensors  
195 per diameter class on trees with the median diameter. Also, before installation, I extracted a 5  
196 mm diameter tree core and stained the sapwood with indicator dye to measure its thickness and  
197 calculate the sapwood area. Sensors were installed following manufacturer instructions ([Burgess](#)  
198 [and Downey, 2014](#)) at diameter breast height.

199 I measured heat velocity every 10 minutes in each tree between May and August 2020. Data  
200 were recorded with the onboard logger of each sensor device. Velocity was measured in two points  
201 across the 35 mm long needle to capture any variability within the sapwood. I then calculated sap  
202 velocity after correcting for tree wounding during installation. Before further processing, I also  
203 corrected sap velocities data for offset due to needle misalignment. To calculate the offset for  
204 each tree and each of the two measurement points along the needle, I calculated the mean sap

205 velocity across the measurement period for nights when the vapour pressure deficit was close to  
206 zero. Sap flow was then calculated for each tree from the sapwood area split into two annuli based  
207 on the measurement depth of each point along the 35 mm needle ([Burgess and Downey, 2014](#)). If  
208 the sapwood area was larger, and there was a leftover area unaccounted for, I linearly interpolated  
209 the inner point sap flow until it reached zero at the end of the sapwood. Due to technical issues,  
210 six of the ten trees gave good quality data during the measurement period.

### 211 **2.2.2 Eddy covariance and meteorology**

212 Evapotranspiration from the eddy covariance flux tower was calculated from changes in atmo-  
213 spheric water concentration and vertical wind speeds. An infra-red gas analyser (LI7500, Li-Cor  
214 Inc., Lincoln NE, USA) and a three-dimensional sonic anemometer (CSAT-3, Campbell Scientific  
215 Ltd., UK) were set up 33 m above ground between 2015 and 2018 and 38 m between 2019 and  
216 2020. Data were logged on a CR3000 (Campbell Scientific Ltd., UK) data logger with a frequency  
217 of 10 Hz. In addition, air temperature, relative humidity (HMP60, Campbell Scientific Ltd., UK)  
218 and precipitation (RG2 rain gauge, Delta-T Devices Ltd., UK) were measured every 5 s from the  
219 top of the tower and aggregated into 30-minutes to match flux data. Global and net radiation  
220 were also measured at the top of the tower with a four-component net radiometer (CNR4, Kipp &  
221 Zonen, Netherlands). For a detailed description of the equipment, set-up, data processing, and  
222 corrections, see [Xenakis et al. \(2021\)](#).

### 223 **2.2.3 Soil water content**

224 The soil water content for each of the ten trees was monitored with CS650 time-domain reflec-  
225 tometry sensors (Campbell Scientific Ltd., UK). The sensors were placed vertically into the soil  
226 surface, approximately 20 cm away from the stem of each tree, and data were recorded with a  
227 CR1000 data logger (Campbell Scientific Ltd., UK). The length of the sensor is 30 cm, so we can  
228 assume values are the mean soil moisture of this depth. For ecosystem level calculations, I used  
229 the mean soil moisture from six CS605 sensors (Campbell Scientific Ltd., UK) placed in a vertical  
230 direction every 5 m along a transect starting from the foot of the tower ([Xenakis et al., 2021](#)).

231 **2.2.4 SAPFLUXNET**

232 I used data from the SAPFLUXNET database version 0.1.5 ([Poyatos et al., 2021](#)). It contains 202  
233 timeseries for 174 tree species. In addition, the database is accompanied by the `sapfluxnetr` R  
234 package, which allows accessing and extracting data and metadata at different temporal scales.

235 For this study, I focused on five biomes: temperate forests, temperate grassland deserts, trop-  
236 ical forest savannas, tropical rainforests, and woodland/shrublands. I extracted daily sapwood-  
237 based time series of sap flow, soil moisture, air temperature and humidity, and soil texture in-  
238 formation for each forest type. Sites with no soil moisture data or soil texture information were  
239 excluded from the analysis. Sites were included irrespective of their experimental treatment. The  
240 final dataset contained time series from 71 sites across 20 countries.

241 **2.3 Additional calculations and analysis**

242 I calculated soil conductivity using generalised soil characteristics equations ([Saxton et al., 1986](#))  
243 and soil texture. Sand and clay for Harwood Forest were set to 40% and 15%, respectively,  
244 following calibration of the process-based model 3PG-SoNWaL to the same volumetric soil water  
245 content data ([Morris et al., 2023](#), in preparation). Soil conductivity for the SAPFLUXNET sites  
246 was also estimated using [Saxton et al. \(1986\)](#). If sand and clay percentage was missing from  
247 each site's metadata, a default value was set using each site's soil texture description. The default  
248 value was the mid-point for each soil texture description in the USDA soil texture classification  
249 triangle ([USDA, 1987](#)). The site was excluded from the analysis if the soil texture description was  
250 also missing. Similarly, soil water potential was also calculated using the generalised equations of  
251 [Saxton et al. \(1986\)](#) from volumetric water content for all three scales.

252 Before further analysis to assess when and for how long trees are likely to experience water  
253 stress, it was crucial to set some theoretical hydraulic efficiency thresholds. Using ECT's maxi-  
254 mum power transfer concept and the response function between  $\eta$  and the ratio of plant to soil  
255 resistance ( $R_{\text{plant}}/R_{\text{soil}}$ ), I chose four thresholds (see results and discussion) to define five zones  
256 of water transport. After calculating  $\eta$  for all datasets, I calculated the empirical cumulative distri-  
257 bution function (ECDF) using the `ecdf` function of the `ggplot2` package and plotted it against  
258 the efficiency. From the intersection between the ECDF and the four  $\eta$  thresholds, I calculated  
259 the total percentage of tree and ecosystem level measurements within each water transport zone.

260 Multiplying the percentage with the total number of days of the sample collection gave the duration  
261 in each category. Finally, for the SAPFLUXNET sites, the mean  $\eta$  per species was calculated and  
262 plotted against the five categories to assess each species' overall hydraulic efficiency.

## 263 3 Results and discussion

### 264 3.1 Thresholds of hydraulic efficiency zones

265 By its definition, the new ECT-based hydraulic efficiency is a dimensionless quantity of the bal-  
266 ance between the transpirational demand and soil water supply (Sperry and Love, 2015). The  
267 advantage is its inherent optimisation point, known as the Maximum Power Transfer (MPT, Figure  
268 3), where plant xylem and soil conductance are equal and  $R_{\text{plant}}/R_{\text{soil}} = 1$ . The second advantage  
269 is that MPT can be identified from timeseries data using widely available sap flow meters and soil  
270 water potential/content sensors.

271 The response function suggests that when  $R_{\text{plant}}/R_{\text{soil}} > 1$ , the water supply is greater than  
272 transpiration. Similarly, when  $R_{\text{plant}}/R_{\text{soil}} < 1$ , water loss exceeds supply. We can then assign  $\eta$   
273 thresholds for defining efficiency zones. At the point of MPT, the response function shows that  $\eta$   
274 = 0.5. Starting from there and allowing a 30% variation on both sides, I defined the "*most efficient*"  
275 water transport zone ( $\eta_{me}$ ) with an efficiency of  $0.412 < \eta \leq 0.565$ . The 30% on either side of MPT  
276 is a reasonable assumption that allows the slope of the hydraulic efficiency function within the most  
277 efficient zone to reflect water balance, as presented in the stomatal optimisation model by Sperry  
278 et al. (2017). Their model assumes that stomata maintain optimum transpiration when canopy  
279 pressure is such that both carbon gain and soil water supply are in balance (Sperry et al., 2017,  
280 Figure 1b). Assuming this is the maximum power transfer point for water movement, deviating  
281 30% has similar implications on water transport, with a decrease suggesting stomatal limitation  
282 and lower transpiration due to lower water supply. I then defined the zone of "*potential water stress*"  
283 with  $\eta \leq 0.412$  ( $\eta_s$ ). On the other hand, I considered the point when soil water conductivity is three  
284 times the plant conductivity as the natural point when the slope of the response function becomes  
285 small that we can consider water supply as unrestricted. The zone when  $0.565 < \eta \leq 0.75$  I  
286 defined as *moderately efficient* water transport ( $\eta_{mu}$ ), with anything between  $0.75 < \eta \leq 0.89$  as  
287 "*moderately unrestricted*" zone. For  $\eta > 0.89$ , I considered it as "*unrestricted*" water supply ( $\eta_u$ ).

288 The hydraulic efficiency zones are not equidistant but dependent on the slope of the response  
289 function (Figure 3). The response function shows a sharp decline in efficiency within the wa-  
290 ter stress zone, suggesting that when efficiency drops below 30% of MPT, transpiration driven  
291 by high vapour pressure deficit increases to such an extent that soil water is depleted rapidly.  
292 Eventually, as the soil dries, transpiration seizes, resulting in no water movement; hence  $\eta = 0$ .  
293 Theoretical work on demand/supply (Sperry and Love, 2015; Sperry et al., 2017) strongly support  
294 my proposed hydraulic efficiency theory under water stress conditions. Sperry and Love (2015),  
295 using a supply/loss theory, showed a sharp decline in transpiration as the soil dried. Sperry et al.  
296 (2017) developed the theory further. They identified the optimum stomatal point when water sup-  
297 ply and carbon gain are in balance, which confirms the maximum power transfer as the point  
298 of optimal stomatal regulation and efficient water movement. Although the hydraulic efficiency I  
299 present here does not inherently include photosynthetic capacity, Sperry et al. (2017) findings sug-  
300 gest that optimal carbon gain must be achieved during MPT. It also explains what the water stress  
301 zone of hydraulic efficiency represents. As canopy pressure increases, xylem water movement  
302 increases, with stomatal being the limiting factor despite the high carbon gain until a critical point  
303 is reached when vulnerability to cavitation increases. Continuing transpiring at high rates will lead  
304 to a drop in soil water availability and hydraulic efficiency. Based on this theory, maximum stomatal  
305 conductance is achieved within the water stress zone. The close theoretical basis between the  
306 ECT-based hydraulic efficiency and the supply/loss theory of Sperry and Love (2015) and Sperry  
307 et al. (2017) increases my confidence in its use as a reliable water stress index. The advantage of  
308 my method is its simplicity, which allows continuous, non-destructive and real-time monitoring of  
309 water stress and the optimum water conditions for growth.

310 Although the theoretical basis of this new water stress index is robust, further work is needed to  
311 establish it as the methodology for answering some fundamental questions regarding the impacts  
312 of water stress and future drought events. For example, it is known that prolonged exposure to  
313 water-limited conditions increases the probability of embolism (Arend et al., 2021), leading to mor-  
314 tality (Choat et al., 2018; Rowland et al., 2015). However, more information is needed about the  
315 minimum length of water stress or how many water-limited periods trees must experience before  
316 critical limitations to growth or mortality. Water manipulation experiments combining measure-  
317 ments of hydraulic efficiency and plant physiological traits (e.g., photosynthetic capacity or water

318 use efficiency) will confirm when water stress occurs, how strong or how long it lasts, and ultimately help us understand if water limitation or carbon starvation is the primary driver of mortality.

### 320 3.2 Tree level

321 The simplistic but robust theoretical basis on ECT of the new hydraulic efficiency makes it applicable at different scales. At the tree level, it is helpful to highlight water stress periods and quantify their length. Figure 4 shows the sap flow, soil water and hydraulic efficiency for three of the six sample trees monitored at Harwood Forest between the end of May and mid-August. I present these three trees as an exemplar of efficiency levels due to the magnitude of transpiration and soil water levels.

327 Tree number 2 had the greatest sapwood area of the three, with  $826.02 \text{ cm}^2$ , followed by trees 9 and 5, with  $412.65$  and  $363.33 \text{ cm}^2$ , respectively. The high sapwood area meant tree 2 transpired up to  $8 \text{ L hr}^{-1}$  after a rainfall event between the 4 and 14 of July replenished the soil water reservoir (Figure 5b). The increase in transpiration after the rainfall was driven by an increase in vapour pressure deficit (Figure 5a). Before the rainfall event, transpiration reduced soil water content for all three trees but at different levels with approximately 30, 20 and 10% minimum  $\theta$  for trees 5, 2 and 9, respectively. The difference in soil water content is because of their location within the stand. Tree 5 was in a flat, less well-drained part of the stand, tree 2 was on a slope of about  $1^\circ$ , and tree 9 was close to a gap in the canopy. For tree 5, the combination of low transpiration and flat terrain must have resulted in the high soil water content. For tree 2, the slope must have contributed to the soil water status. However, for tree 9, the gap must have allowed more light into the ground, increasing the evaporation and transpiration components and resulting in lower soil availability. The magnitude of measured sap flow in this study was typical for Sitka spruce. Beauchamp et al. (2013) found sap flow of a Sitka spruce tree with a similar sapwood area to tree 9 ( $418.62 \text{ cm}^2$ ) picked at  $4.3 \text{ L hr}^{-1}$  during August, very close to the value of  $4 \text{ L hr}^{-1}$  found here.

343 Calculations of the hydraulic efficiency showed that tree 5 did not experience any water stress throughout the sampling period. Hence its water transport was efficient although small ( $2\text{-}4 \text{ L hr}^{-1}$ ). Out of the three, tree 9 experienced greater water stress with a prolonged period of  $\eta$  being close to zero (Figure 4). Both trees 2 and 9 experienced water stress prior to the rainfall

event, with tree 9 experiencing it much faster (Figure 6). During the rainfall event, efficiency increased due to high water availability and low transpiration, meaning water movement, although small, was unrestricted. After the rainfall event, efficiency started to drop again, getting closer to the moderate and most efficient zones for both trees 2 and 9. Noticeable, however, is how quickly tree 9 returns to the water stress zone after the rainfall event despite soil water going up to about 22%. [Xenakis et al. \(2021\)](#) found that the average soil moisture for the stand during the extreme drought of 2018 was 23%. Soil water around tree 9 seemed to be below the average of a drought period, which suggests, despite the high rates of transpiration (4-6 L hr<sup>-1</sup>), the tree is experiencing prolonged water stress conditions and hence more likely to suffer from either catastrophic xylem failure ([Arend et al., 2021](#); [Brodribb and Cochard, 2009](#); [McDowell et al., 2008](#)) under extreme water limitation such as this experiences by the tree during the 2018 drought.

The radial distribution of sap flow differed between the three trees (Figure 7). Sap flow in tree 5 was evenly distributed in the outer and inner sections of the sapwood. On the other hand, tree 9 was found to have a higher flow on the inner section, which indicates water stress. [Hernandez-Santana et al. \(2013\)](#), in their study with young olive trees, also showed that during periods of high water deficit, the inner section of the xylem had a greater contribution to the total flow of sap. Their findings confirm that tree 9 suffered water stress and supports my ECT-based conclusion. This also increases my confidence in hydraulic efficiency as a reliable water stress indicator.

We can also assess the total time spent under stress conditions with ECT-based hydraulic efficiency. To this end, we can use empirical cumulative density functions (Figure 6). I found that for almost 70% of the monitoring period, tree 9 showed an efficiency of less than 0.1, with 82% within the water stress zone, that is, 67 out of 82 days of monitoring (Table 2). Tree 2 was only 15 days in the water stress zone (18.4% of the sampling period). Both trees spend two to three days in the most efficient water transport zone (Table 2). On the other hand, tree 2 was 49 days in the unrestricted water transport zone, while tree 9 was only seven days. Out of the six trees monitored, four were more than 50% of the time within the unrestricted water transport zone and had a mean  $\eta$  of more than 75% (Table 2). The organo-mineral peaty gley soil keeps high water levels preventing trees from being within the most efficient water transport zone. Soil trenching during stand establishment traditionally aims to reduce soil moisture levels ([Butler et al., 2010](#)). My analysis showed that draining would reduce soil water and allow the water flow within SPA to

377 become more efficient. Under future climatic drought, Sitka spruce is expected to become very  
378 quickly water stressed because of its slow stomatal response (Beadle et al., 1978). Continuing  
379 drying wet sites will add to the drop in hydraulic efficiency. The establishment of continuous  
380 monitoring of hydraulic efficiency can target management decisions aiming to maximise soil water  
381 levels based on tree-level demands. Monitoring hydraulic efficiency during in-situ experiments  
382 manipulating water levels can also help collect the data to understand further the growth impact  
383 on achieving the most efficient hydraulic flow through the SPA.

### 384 3.3 Ecosystem level

385 Hydraulic efficiency calculated at the ecosystem level using six years of eddy covariance data  
386 showed evident water stress during 2018 (Figure 8). The stand was in the water stress zone for  
387 115 days (31% of the year) and 143 (40% of the year) in the unrestricted water transport zone  
388 (Table 2). During 2018, the stand spent 9% of the year in the most efficient zone, the highest out  
389 of the six years.

390 Water transport became more efficient for 32 days as the site was drying. However, as the site  
391 continued to dry, it entered a prolonged water stress period that resulted in 7% less photosynthesis  
392 and a drop in inherent water use efficiency by 73% compared to the previous three years (Xenakis  
393 et al., 2021). In the following two years, the stand spent less time under water stress conditions  
394 which helped the recovery of the photosynthesis to 2015 levels (data not shown). However, despite  
395 the two-year post-drought recovery of photosynthesis due to the high vapour pressure deficit of  
396 2018 (Aubinet et al., ???), the site did not recover to its usual pre-drought water balance (Figure  
397 8b).

398 The annual ECDF analysis of the hydraulic efficiency with the results by Xenakis et al. (2021)  
399 showed that Sitka spruce achieved high levels of photosynthesis ( $23 - 25 \text{ tC ha}^{-1}$ ) under unre-  
400 stricted water availability. However, when the stand was under water stress for a third of the year,  
401 there was a significant drop in carbon uptake and water use efficiency, despite the small drop in  
402 photosynthesis. This has implications for the growth and its use for fulfilling national net zero tar-  
403 gets under future climate (Bateman et al., 2022), where droughts will become more frequent and  
404 water resources more sparse (Zhou et al., 2019). Less precipitation will mean less soil water, and  
405 a warmer climate will increase vapour pressure deficit and transpiration. It is unknown how pho-

406 tosynthesis will respond to more balanced water uptake. We must continue our investigations and  
407 monitoring using either existing eddy covariance flux sites or manipulation experiments to better  
408 understand the impacts of water limitation.

#### 409 3.4 Biome level

410 Drought-related research focuses on understanding the mechanisms developed by trees to man-  
411 age available water resources cost-effectively ([Martínez-Vilalta et al., 2014](#); [Mencuccini et al.,](#)  
412 [2019](#); [Sperry and Love, 2015](#); [Sperry et al., 2017](#)). Analysis of global datasets often offers a  
413 broader range of variability, helping conclude fundamental water regulation mechanisms within  
414 the soil-plant continuum. My focus, however, when looking at the biome level is to answer a fun-  
415 damentally more important question. Which species offers the most efficient water management  
416 mechanisms. The implication is that less efficient species may suffer under water stress since  
417 there was limited natural adaptation time due to an accelerated change in the climate. Currently,  
418 net zero emission policies require forest expansion but minimising the risk of tree mortality due  
419 to drought. Hence, we must focus on identifying species that can handle limited water resources  
420 more efficiently across all climatic zones.

421 Here, I applied my new method of assessing the hydraulic efficiency for a wide range of species  
422 across five biome types. Figure 9 illustrates the mean  $\eta$ . The analysis showed that most forest  
423 species in the temperate zone had  $\eta$  more than 0.75. Two species were most efficient in water  
424 transport, and five were under stress. On the other hand, most tropical forest savanna species  
425 were within the water stress zone.

426 The mean efficiency of Sitka spruce was in the unrestricted hydraulic efficiency zone, which  
427 confirms my ecosystem-level findings. It grows in wet soil conditions with transpirational losses  
428 rarely exceeding available water. The mean hydraulic efficiency for beech in the temperature zone  
429 was within the moderately unrestricted zone and in the unrestricted zone as woodland/shrubland.  
430 Similarly, Scots pine as a temperate forest had moderately efficient water transport, whereas  
431 woodland was moderately unrestricted, demonstrating that climate zone and management can  
432 affect water transport through the SPA. I also found that Aleppo pine and holm oak, two species  
433 widely found in the Mediterranean region, are most efficient in managing water resources, con-  
434 firming adaptation strategies for efficient water regulation, which is important for survival in water-

435 limiting environments.

436 The implication of this global analysis is twofold. First, it allows one to assess and compare  
437 the species and gain insights into water management strategies. Second, and more crucially, it  
438 allows the evaluation of alternative species for adaptation of forest plantations under future climate.  
439 So far, our understanding of species water management strategies was based on experiments,  
440 monitoring studies or expert knowledge. Standardised databases such as SAPFLUXNET allow for  
441 exploring a wider range of species and evaluating the best water management strategy. Species  
442 with high  $\eta$  are those with levels of transpiration that rarely exceed the available soil water and  
443 hence very unlikely to have experienced water stress. From an evolutionary perspective, these  
444 species have little time to develop the mechanisms to reduce their vulnerability to drought and  
445 hence will not make the best option for future adaptation.

446 To improve upon such global analysis, ECT-based hydraulic efficiency needs to be linked  
447 more strongly to elements of photosynthesis, carbon uptake and growth. Furthermore, it needs to  
448 consider resource competition when trees are in mixtures or even uneven-canopy structures.

### 449 3.5 Further discussion

450 An important element when considering water movement within plants is stem water storage,  
451 which is analogous to capacitance ([Zhuang et al., 2014](#)). It is known that capacitance contributes  
452 to transpiration during water stress periods, which can be between 2 and 5% [Salomón et al.](#)  
453 ([2017](#)). Capacitance, however, is not included in my analogy. Electrical circuits analogies of  
454 water plant movement are commonly open circuits, with several resistors representing plant parts  
455 (e.g., roots, stem, branches and leaves, [Landsberg et al., 1976](#); [Milne et al., 1983](#); [Hunt et al.](#),  
456 [1991](#)) and with two points of potential difference, soil and leaf. The difference with my analogy  
457 is that it is a close circuit with the plant depicted as a single resistance. At the same time, the  
458 soil is represented not only by a potential but also a resistance. So, the contribution of the stem  
459 capacitance is inherently part of the plant resistor.

460 The single resistance based on stem conductivity is a reasonable assumption for large trees.  
461 Data by [Landsberg et al. \(1976\)](#) comparing the resistance of root and stem in two-year-old young  
462 apple trees showed that stem resistance was 34% of the total stem and root resistance. However,  
463 for nine-year-old trees, stem resistance increased to 50%. Hence, stem resistance is expected to

464 increase as trees grow, which validates my assumption. In this study, my focus was on mature  
465 trees. Therefore, we must further test and validate the theory and its assumptions on younger  
466 trees. Nevertheless, the data I presented here increased my confidence that the theoretical basis  
467 is sound and robust.

468 To my knowledge, no previous definition considers how efficiently water is transported through  
469 the SPA. This makes the definition of hydraulic efficiency I presented in this study unique. Although  
470 it uses simple concepts of electric theory in its basis, I do not consider it uniquely different from the  
471 theoretical framework set by [Sperry and Love \(2015\)](#) and [Sperry et al. \(2017\)](#) or the arguments  
472 raised by [Anderegg et al. \(2012\)](#) regarding the use of water deficit to define when drought-induced  
473 mortality occurs. All these approaches follow the fundamental principle of finding the balance point  
474 between input and output, supply and loss, or Maximum Point Transfer. So, although supply/loss  
475 theory is a good insight into the underline physiological processes, ECT-based hydraulic efficiency  
476 offers a methodological simplification for a more relevant practical and wider application, allowing  
477 finer granularity both in space and time.

478 On that end, ECT-based hydraulic efficiency is easily transferable and applicable for large-  
479 scale monitoring of forest drought using modern technology, specifically Internet of Things de-  
480 vices. The increase in cost-effectiveness of such devices, and the construction of robust sensors  
481 that collect soil and transpiration data, allow long-term and wider deployment across areas with  
482 sufficient network connectivity. Live data streaming and online processing using my theory will of-  
483 fer a real-time water monitoring system, where the impact of decisions on water balance, such as  
484 species, silvicultural system or management intervention (e.g., drainage, irrigation) can be mon-  
485 itored. Moreover, the continuous monitoring of hydraulic efficiency, when combined with other  
486 continuous measurements such as dendrometry ([Bourbia and Brodribb, 2023](#)) or water stable iso-  
487 topes ([Marshall et al., 2020](#)), offers a great opportunity for monitoring how water stress affects  
488 photosynthesis and growth during naturally occurring droughts or via large water exclusion ex-  
489 periments. Furthermore, global datasets such as those offered by SAPFLUXNET, FLUXNET, and  
490 ICOS offer the possibility of assessing the hydraulic efficiency of different ecosystems and species  
491 and looking further into water stress impacts on carbon uptake. The application of hydraulic effi-  
492 ciency can extend even further into process-based modelling. Integration with either detailed mod-  
493 els of water transport or more simplistic yet drought-sensitive models such as the 3PG-SoNWaL

494 model (Morris et al., 2023, in preparation) will offer the data for a probabilistic drought risk as-  
495 sessment (Oijen and Zavala, 2019) based on SPA water balance. Finally, ECT-based hydraulic  
496 efficiency has great potential for large-scale applications using remote sensing. Recent devel-  
497 opments in the improvement of radar backscatter have the potential to offer a quantification of  
498 above-canopy evapotranspiration losses and below-canopy soil moisture. In addition, improving  
499 soil texture maps can significantly improve estimates of hydraulic efficiency at large scales.

## 500 4 Conclusions

501 When dealing with the impact of climate change-induced water stress on forest resources, efforts  
502 concentrate on understanding what causes water stress, how trees deal with it and what mecha-  
503 nisms they use to adapt and avoid mortality. However, further from understanding the fundamental  
504 principles, we require a reliable monitoring water stress system for early detection. Because re-  
505 silience is based on understanding the timing, duration, and impact of stresses, it is imperative to  
506 develop a system with a sound theoretical basis that provides robust predictions and allows easy  
507 application. Electric Circuit Theory, as I demonstrated, offers all three. Using the definition of hy-  
508 draulic efficiency I proposed here, we saw when water is most efficiently transported through the  
509 SPA (Figure 4) and how long they have been under water stress (Table 2). Moreover, using ECT,  
510 we found the spruce stand was under drought conditions for a third of a year. Finally, we saw how  
511 the same species differ in how they transport water in different biomes. Moreover, I demonstrated  
512 a method for comparing species based on their water transport. Now that the fundamental prin-  
513 ciples are set, we must use them to further advance our understanding of the impact of longevity  
514 and frequent water stress events not only on mortality but on the reduction of productivity and the  
515 ability to regulate water balance at either the tree or ecosystem level.

## 516 References

- 517 Alizadeh, A., Toudestki, A., Ehsani, R., Migliaccio, K., Wang, D., 2021. Detecting tree water  
518 stress using a trunk relative water content measurement sensor. Smart Agricultural Technology  
519 1, 100003.  
520 URL <https://doi.org/10.1016/j.atech.2021.100003>

- 521 Anderegg, W. R., Berry, J. A., Field, C. B., 12 2012. Linking definitions, mechanisms, and modeling  
522 of drought-induced tree death. *Trends in Plant Science* 17, 693–700.
- 523 URL <https://linkinghub.elsevier.com/retrieve/pii/S1360138512002130>
- 524 Arend, M., Link, R. M., Patthey, R., Hoch, G., Schuldt, B., Kahmen, A., 4 2021. Rapid hydraulic col-  
525 lapse as cause of drought-induced mortality in conifers. *Proceedings of the National Academy*  
526 of Sciences of the United States of America
- 527 URL <https://www.pnas.org/doi/abs/10.1073/pnas.2025251118>
- 528 Aubinet, M., Hurdebié, Q., Chopin, H., Debacq, A., Ligne, A. D., Heinesch, B., Manise, T., Vincke,  
529 C., ???? [inter-annual variability of net ecosystem productivity for a temperate mixed forest: A  
530 predominance of carry-over effects? *Agricultural and Forest Meteorology*, 340–353.
- 531 Bateman, I. J., Anderson, K., Argles, A., Belcher, C., Betts, R. A., Binner, A., Brazier, R. E., Cho, F.  
532 H. T., Collins, R. M., Day, B. H., Duran-Rojas, C., Eisenbarth, S., Gannon, K., Gatis, N., Groom,  
533 B., Hails, R., Harper, A. B., Harwood, A., Hastings, A., Heard, M. S., Hill, T. C., Inman, A., Lee,  
534 C. F., Luscombe, D. J., MacKenzie, A. R., Mancini, M. C., Morison, J. I. L., Morris, A., Quine,  
535 C. P., Snowdon, P., Tyler, C. R., Vanguelova, E. I., Wilkinson, M., Williamson, D., Xenakis, G.,  
536 5 2022. A review of planting principles to identify the right place for the right tree for ‘net zero  
537 plus’ woodlands: Applying a place-based natural capital framework for sustainable, efficient and  
538 equitable (SEE) decisions. *People and Nature*.
- 539 URL <https://onlinelibrary.wiley.com/doi/10.1002/pan3.10331>
- 540 Beadle, C. L., Turner, N. C., Jarvis, P. G., 1978. Critical water potential for stomatal closure in Sitka  
541 spruce. *Physiologia Plantarum* 43, 160–165.
- 542 Beauchamp, K., Mencuccini, M., Perks, M., Gardiner, B., 2013. The regulation of sapwood area,  
543 water transport and heartwood formation in Sitka spruce. *Plant Ecology and Diversity* 6, 45–56.
- 544 Bourbia, I., Brodribb, T. J., 3 2023. A new technique for monitoring plant transpiration under field  
545 conditions using leaf optical dendrometry. *Agricultural and Forest Meteorology* 331, 109328.
- 546 URL <https://linkinghub.elsevier.com/retrieve/pii/S0168192323000229>
- 547 Brodribb, T. J., Cochard, H., 2009. Hydraulic failure defines the recovery and point of death in  
548 water-stressed conifers. *Plant Physiology* 149, 575–584.

- 549 Burgess, S., Downey, A., 5 2014. SFM1 Sap Flow Meter Manual.
- 550 Burgess, S. S., Adams, M. A., Turner, N. C., Beverly, C. R., Ong, C. K., Khan, A. A., Bleby, T. M.,  
551 2001. An improved heat pulse method to measure low and reverse rates of sap flow in woody  
552 plants. *Tree Physiology* 21, 589–598.
- 553 Butler, A. J., Barbier, N., Čermák, J., Koller, J., Thornily, C., McEvoy, C., Nicoll, B., Perks, M. P.,  
554 Grace, J., Meir, P., 6 2010. Estimates and relationships between aboveground and belowground  
555 resource exchange surface areas in a Sitka spruce managed forest. *Tree Physiology* 30, 705–  
556 714.
- 557 URL <https://academic.oup.com/treephys/article/30/6/705/1616157>
- 558 Carminati, A., Javaux, M., 2020. Soil Rather Than Xylem Vulnerability Controls Stomatal Re-  
559 sponse to Drought. *Trends in Plant Science* 25, 868–880.
- 560 URL <https://doi.org/10.1016/j.tplants.2020.04.003>
- 561 Charra-Vaskou, K., Badel, E., Burlett, R., Cochard, H., Delzon, S., Mayr, S., 2012. Hydraulic  
562 efficiency and safety of vascular and non-vascular components in *Pinus pinaster* leaves. *Tree  
563 Physiology* 32, 1161–1170.
- 564 Choat, B., Brodribb, T. J., Brodersen, C. R., Duursma, R. A., López, R., Medlyn, B. E., 2018.  
565 Triggers of tree mortality under drought. *Nature* 558, 531–539.
- 566 Choat, B., Jansen, S., Brodribb, T. J., Cochard, H., Delzon, S., Bhaskar, R., Bucci, S. J., Feild,  
567 T. S., Gleason, S. M., Hacke, U. G., Jacobsen, A. L., Lens, F., Maherli, H., Martínez-Vilalta, J.,  
568 Mayr, S., Mencuccini, M., Mitchell, P. J., Nardini, A., Pittermann, J., Pratt, R. B., Sperry, J. S.,  
569 Westoby, M., Wright, I. J., Zanne, A. E., 11 2012. Global convergence in the vulnerability of  
570 forests to drought. *Nature* 491, 752–755.
- 571 URL <http://www.nature.com/articles/nature11688>
- 572 Ciruzzi, D. M., Loheide, S. P., 11 2019. Monitoring tree sway as an indicator of water stress.  
573 *Geophysical Research Letters* 46, 12021–12029.
- 574 Conejero, W., Alarcón, J. J., García-Orellana, Y., Abrisqueta, J. M., Torrecillas, A., 1 2007. Daily  
575 sap flow and maximum daily trunk shrinkage measurements for diagnosing water stress in early

- 576 maturing peach trees during the post-harvest period. *Tree Physiology* 27, 81–88.
- 577 URL <https://academic.oup.com/treephys/article/27/1/81/1674535>
- 578 Dickson, B. G., Albano, C. M., Anantharaman, R., Beier, P., Fargione, J., Graves, T. A., Gray, M. E.,  
579 Hall, K. R., Lawler, J. J., Leonard, P. B., Littlefield, C. E., McClure, M. L., Novembre, J., Schloss,  
580 C. A., Schumaker, N. H., Shah, V. B., Theobald, D. M., 2018. Circuit-theory applications to  
581 connectivity science and conservation. *Conservation Biology* 0, 1–11.
- 582 URL [www.circuitscape.org](http://www.circuitscape.org)
- 583 Drechsler, K., Kisekka, I., Upadhyaya, S., 5 2019. A comprehensive stress indicator for evaluating  
584 plant water status in almond trees. *Agricultural Water Management* 216, 214–223.
- 585 Feiziasl, V., Jafarzadeh, J., Sadeghzadeh, B., Shalmani, M. A. M., 3 2022. Water deficit index to  
586 evaluate water stress status and drought tolerance of rainfed barley genotypes in cold semi-arid  
587 area of Iran. *Agricultural Water Management* 262.
- 588 Fuchs, S., Leuschner, C., Link, R. M., Schuldt, B., 2021. Hydraulic variability of three temperate  
589 broadleaf tree species along a water availability gradient in central Europe. *New Phytologist*  
590 231, 1387–1400.
- 591 Granier, A., Loustau, D., Bréda, N., 12 2000. A generic model of forest canopy conductance  
592 dependent on climate, soil water availability and leaf area index. *Annals of Forest Science* 57,  
593 755–765.
- 594 URL <http://www.edpsciences.org/10.1051/forest:2000158>
- 595 Grossiord, C., Buckley, T. N., Cernusak, L. A., Novick, K. A., Poulter, B., Siegwolf, R. T. W., Sperry,  
596 J. S., McDowell, N. G., 6 2020. Plant responses to rising vapor pressure deficit. *New Phytologist*  
597 226, 1550–1566.
- 598 URL <https://onlinelibrary.wiley.com/doi/10.1111/nph.16485>
- 599 Han, M., Zhang, H., DeJonge, K., Comas, L., Gleason, S., 2018. Comparison of three crop water  
600 stress index models with sap flow measurements in maize. *Agricultural Water Management* 203,  
601 366–375.
- 602 Hernandez-Santana, V., Alvarado-Barrientos, M., Rodriguez-Dominguez, C., Perez-Martin, A.,  
603 Diaz-Espejo, A., 5 2013. Linking changes in radial profiles of sap flux density with the response

- 604 of water vapour exchange to water deficit. *Acta Horticulturae*, 189–196.
- 605 URL [https://www.actahort.org/books/991/991\\_23.htm](https://www.actahort.org/books/991/991_23.htm)
- 606 Hunt, E. R., Running, S. W., Federer, C. A., 1991. Extrapolating plant water flow resistances and  
607 capacitances to regional scales. *Agricultural and Forest Meteorology* 54, 169–195.
- 608 Jones, H. G., 1992. Plants and microclimate: A quantitative approach to environmental plant  
609 physiology. Cambridge University Press.
- 610 Knüsel, S., Peters, R. L., Haeni, M., Wilhelm, M., Zweifel, R., 2021. Processing and extraction of  
611 seasonal tree physiological parameters from stem radius time series. *Forests* 12, 1–14.
- 612 Konings, A. G., Saatchi, S. S., Frankenberg, C., Keller, M., Leshyk, V., Anderegg, W. R., Humphrey,  
613 V., Matheny, A. M., Trugman, A., Sack, L., Agee, E., Barnes, M. L., Binks, O., Cawse-Nicholson,  
614 K., Christoffersen, B. O., Entekhabi, D., Gentine, P., Holtzman, N. M., Katul, G. G., Liu, Y., Longo,  
615 M., Martinez-Vilalta, J., McDowell, N., Meir, P., Mencuccini, M., Mrad, A., Novick, K. A., Oliveira,  
616 R. S., Siqueira, P., Steele-Dunne, S. C., Thompson, D. R., Wang, Y., Wehr, R., Wood, J. D., Xu,  
617 X., Zuidema, P. A., 12 2021. Detecting forest response to droughts with global observations of  
618 vegetation water content. *Global Change Biology* 27, 6005–6024.
- 619 Kramp, R. E., Liancourt, P., Herberich, M. M., Saul, L., Weides, S., Tielbörger, K., Májeková, M., 9  
620 2022. Functional traits and their plasticity shift from tolerant to avoidant under extreme drought.  
621 Ecology.
- 622 URL <https://onlinelibrary.wiley.com/doi/10.1002/ecy.3826>
- 623 Landsberg, J. J., Blanchard, T. W., Warrit, B., 1976. Studies on the movement of water through  
624 apple trees. *Journal of Experimental Botany* 27, 579–596.
- 625 Losso, A., Challis, A., Gauthey, A., Nolan, R. H., Hislop, S., Roff, A., Boer, M. M., Jiang, M.,  
626 Medlyn, B. E., Choat, B., 12 2022. Canopy dieback and recovery in Australian native forests  
627 following extreme drought. *Scientific Reports* 12, 21608.
- 628 URL <https://www.nature.com/articles/s41598-022-24833-y>
- 629 Marshall, J. D., Cuntz, M., Beyer, M., Dubbert, M., Kuehnhammer, K., 4 2020. Borehole Equili-  
630 bration: Testing a New Method to Monitor the Isotopic Composition of Tree Xylem Water in situ.  
631 Frontiers in Plant Science 11.

- 632 Martínez-Vilalta, J., Poyatos, R., Aguadé, D., Retana, J., Mencuccini, M., 2014. A new look at  
633 water transport regulation in plants. *New Phytologist* 204, 105–115.
- 634 McDowell, N., Pockman, W. T., Allen, C. D., Breshears, D. D., Cobb, N., Kolb, T., Plaut, J., Sperry,  
635 J., West, A., Williams, D. G., Yepez, E. A., 2008. Mechanisms of plant survival and mortality  
636 during drought: Why do some plants survive while others succumb to drought? *New Phytologist*  
637 178, 719–739.
- 638 McRae, B. H., Beier, P., 2007. Circuit theory predicts gene flow in plant and animal populations.  
639 PNAS December 11.
- 640 URL [www.pnas.org/cgi/doi/10.1073/pnas.0706568104](http://www.pnas.org/cgi/doi/10.1073/pnas.0706568104)
- 641 McRae, B. H., Dickson, B. G., Keitt, T. H., Shah, V. B., 2008. Using circuit theory to model connec-  
642 tivity in ecology, evolution, and conservation. *Concepts & synthesis emphasizing new ideas to*  
643 stimulate research in ecology 89, 2712–2724.
- 644 Mencuccini, M., Manzoni, S., Christoffersen, B., 5 2019. Modelling water fluxes in plants: from  
645 tissues to biosphere. *New Phytologist* 222, 1207–1222.
- 646 URL <https://onlinelibrary.wiley.com/doi/10.1111/nph.15681>
- 647 Milne, R., Ford, E., Deans, J., 1983. Time lags in the water relations of sitka spruce. *Forest Ecology*  
648 and Management
- 649 and Management 5, 1–25.
- 649 Morris, A., Xenakis, G., Perks, M., 2023. Developing the drought-sensitive model 3PG-SoNWaL:  
650 evaluating its sensitivity during the 2018 drought for a Sitka spruce stand. In preparation.
- 651 Nackley, L. L., Sousa, E. F. D., Pitton, B. J., Sisneroz, J., Oki, L. R., 2020. Developing a water-  
652 stress index for potted poinsettia production. *HortScience* 55, 1295–1302.
- 653 Nadezhina, N., 1999. Sap flow index as an indicator of plant water status. *Tree Physiology* 19,  
654 885–891.
- 655 Naithani, K. J., Ewers, B. E., Pendall, E., 2012. Sap flux-scaled transpiration and stomatal conduc-  
656 tance response to soil and atmospheric drought in a semi-arid sagebrush ecosystem. *Journal*  
657 *of Hydrology*, 176–185.
- 658 URL <http://dx.doi.org/10.1016/j.jhydrol.2012.07.008>

- 659 Nel, A. A., Berliner, P. R., 1990. Quantifying leaf water potential for scheduling irrigation of wheat  
660 under specific soil-climate conditions. *South African Journal of Plant and Soil* 7, 68–71.
- 661 Nieto, H., Alsina, M., Kustas, W., García-Tejera, O., Chen, F., Bambach, N., Gao, F., Alfieri, J.,  
662 Hipps, L., Prueger, J., Castro, S., Dokoozlian, N., 2022. Evaluating different metrics from the  
663 thermal-based two-source energy balance model for monitoring grapevine water stress. *Irriga-*  
664 *tion Science*.
- 665 Ojen, M. V., Zavala, M. A., 2019. Probabilistic drought risk analysis for even-aged forests. Elsevier,  
666 pp. 159–176.
- 667 Poyatos, R., Granda, V., Flo, V., Adams, M. A., Adorján, B., Aguadé, D., Aidar, M. P. M., Allen, S.,  
668 Alvarado-Barrientos, M. S., Anderson-Teixeira, K. J., Aparecido, L. M., Arain, M. A., Aranda, I.,  
669 Asbjornsen, H., Baxter, R., Beamesderfer, E., Berry, Z. C., Berveiller, D., Blakely, B., Boggs, J.,  
670 Bohrer, G., Bolstad, P. V., Bonal, D., Bracho, R., Brito, P., Brodeur, J., Casanoves, F., Chave,  
671 J., Chen, H., Cisneros, C., Clark, K., Cremonese, E., Dang, H., David, J. S., David, T. S.,  
672 Delpierre, N., Desai, A. R., Do, F. C., Dohnal, M., Domec, J.-C., Dzikiti, S., Edgar, C., Eichstaedt,  
673 R., El-Madany, T. S., Elbers, J., Eller, C. B., Euskirchen, E. S., Ewers, B., Fonti, P., Forner,  
674 A., Forrester, D. I., Freitas, H. C., Galvagno, M., Garcia-Tejera, O., Ghimire, C. P., Gimeno,  
675 T. E., Grace, J., Granier, A., Griebel, A., Guangyu, Y., Gush, M. B., Hanson, P. J., Hasselquist,  
676 N. J., Heinrich, I., Hernandez-Santana, V., Herrmann, V., Hölttä, T., Holwerda, F., Irvine, J.,  
677 Isarangkool Na Ayutthaya, S., Jarvis, P. G., Jochheim, H., Joly, C. A., Kaplick, J., Kim, H. S.,  
678 Klemedtsson, L., Kropp, H., Lagergren, F., Lane, P., Lang, P., Lapenas, A., Lechuga, V., Lee,  
679 M., Leuschner, C., Limousin, J.-M., Linares, J. C., Linderson, M.-L., Lindroth, A., Llorens, P.,  
680 López-Bernal, A., Loranty, M. M., Lütschwager, D., Macinnis-Ng, C., Maréchaux, I., Martin,  
681 T. A., Matheny, A., McDowell, N., McMahon, S., Meir, P., Mészáros, I., Migliavacca, M., Mitchell,  
682 P., Mölder, M., Montagnani, L., Moore, G. W., Nakada, R., Niu, F., Nolan, R. H., Norby, R.,  
683 Novick, K., Oberhuber, W., Obojes, N., Oishi, A. C., Oliveira, R. S., Oren, R., Ourcival, J.-M.,  
684 Paljakka, T., Perez-Priego, O., Peri, P. L., Peters, R. L., Pfautsch, S., Pockman, W. T., Preisler,  
685 Y., Rascher, K., Robinson, G., Rocheteau, A., Röll, A., Rosado, B. H. P., Rowland,  
686 L., Rubtsov, A. V., Sabaté, S., Salmon, Y., Salomón, R. L., Sánchez-Costa, E., Schäfer, K. V. R.,  
687 Schuldt, B., Shashkin, A., Stahl, C., Stojanović, M., Suárez, J. C., Sun, G., Szatniewska, J.,

- 688 Tatarinov, F., Tesař, M., Thomas, F. M., Tor-ngern, P., Urban, J., Valladares, F., van der Tol,  
689 C., van Meerveld, I., Varlagin, A., Voigt, H., Warren, J., Werner, C., Werner, W., Wieser, G.,  
690 Wingate, L., Wullschleger, S., Yi, K., Zweifel, R., Steppe, K., Mencuccini, M., Martínez-Vilalta,  
691 J., 2021. Global transpiration data from sap flow measurements: the SAPFLUXNET database.  
692 Earth System Science Data 13 (6), 2607–2649.
- 693 URL <https://essd.copernicus.org/articles/13/2607/2021/>
- 694 R Core Team, 2022. R: A Language and Environment for Statistical Computing. R Foundation for  
695 Statistical Computing, Vienna, Austria.
- 696 URL <https://www.R-project.org/>
- 697 Rehschuh, R., Cecilia, A., Zuber, M., Faragó, T., Baumbach, T., Hartmann, H., Jansen, S., Mayr,  
698 S., Ruehr, N., 2020. Drought-induced xylem embolism limits the recovery of leaf gas exchange  
699 in Scots pine. Plant Physiology 184, 852–864.
- 700 Reinert, S., Bögelein, R., Thomas, F., 2012. Use of thermal imaging to determine leaf conductance  
701 along a canopy gradient in European beech (*Fagus sylvatica*). Tree Physiology 32, 294–302.
- 702 Rowland, L., Costa, A. C. D., Galbraith, D. R., Oliveira, R. S., Binks, O. J., Oliveira, A. A., Pullen,  
703 A. M., Doughty, C. E., Metcalfe, D. B., Vasconcelos, S. S., Ferreira, L. V., Malhi, Y., Grace, J.,  
704 Mencuccini, M., Meir, P., 2015. Death from drought in tropical forests is triggered by hydraulics  
705 not carbon starvation. Nature 528, 119–122.
- 706 Salomón, R. L., Limousin, J. M., Ourcival, J. M., Rodríguez-Calcerrada, J., Steppe, K., 2017. Stem  
707 hydraulic capacitance decreases with drought stress: implications for modelling tree hydraulics  
708 in the Mediterranean oak *Quercus ilex*. Plant Cell and Environment 40, 1379–1391.
- 709 Saxton, K. E., Rawls, W. J., Romberger, J. S., Papendick, R. I., 1986. Estimating soil water  
710 characteristics-hydraulic conductivity. Soil Science Society of America Journal 5, 1031–1036.
- 711 Schumann, K., Leuschner, C., Schuldt, B., 10 2019. Xylem hydraulic safety and efficiency in  
712 relation to leaf and wood traits in three temperate *Acer* species differing in habitat preferences.  
713 Trees - Structure and Function 33, 1475–1490.
- 714 Sperry, J. S., Love, D. M., 7 2015. What plant hydraulics can tell us about responses to climate-

- 715 change droughts. *New Phytologist* 207, 14–27.
- 716 URL <https://onlinelibrary.wiley.com/doi/10.1111/nph.13354>
- 717 Sperry, J. S., Venturas, M. D., Anderegg, W. R., Mencuccini, M., Mackay, D. S., Wang, Y., Love,  
718 D. M., 2017. Predicting stomatal responses to the environment from the optimization of photo-  
719 synthetic gain and hydraulic cost. *Plant Cell and Environment* 40, 816–830.
- 720 Tadesse, T., Hollinger, D. Y., Bayissa, Y. A., Svoboda, M., Fuchs, B., Zhang, B., Demissie, G.,  
721 Wardlow, B. D., Bohrer, G., Clark, K. L., Desai, A. R., Gu, L., Noormets, A., Novick, K. A.,  
722 Richardson, A. D., 11 2020. Forest Drought Response Index (ForDRI): A New Combined Model  
723 to Monitor Forest Drought in the Eastern United States. *Remote Sensing* 2020, Vol. 12, Page  
724 3605 12, 3605.
- 725 URL <https://www.mdpi.com/2072-4292/12/21/3605/htm> <https://www.mdpi.com/2072-4292/12/21/3605>
- 726
- 727 Tang, J., Riley, W. J., Marschmann, G. L., Brodie, E. L., 10 2021. Conceptualizing biogeochemical  
728 reactions with an Ohm's law analogy. *Journal of Advances in Modeling Earth Systems* 13.
- 729 USDA, 1987. Soil mechanics level 1, module 3. USDA textural classification study guide.
- 730 van der Sande, M. T., Poorter, L., Schnitzer, S. A., Engelbrecht, B. M., Markestijn, L., 5 2019.  
731 The hydraulic efficiency–safety trade-off differs between lianas and trees. *Ecology* 100.
- 732 Venturin, A. Z., Guimarães, C. M., de Sousa, E. F., Filho, J. A. M., Rodrigues, W. P., Ícaro de  
733 Araujo Serrazine, Bressan-Smith, R., Marciano, C. R., Campostrini, E., 11 2020. Using a crop  
734 water stress index based on a sap flow method to estimate water status in conilon coffee plants.  
735 *Agricultural Water Management* 241, 106343.
- 736 URL <https://linkinghub.elsevier.com/retrieve/pii/S037837741932027X>
- 737 Vido, J., Střelcová, K., Nalevanková, P., Leštiánska, A., Kandrik, R., Pástorová, A., Škvarenina,  
738 J., Tadesse, T., 2016. Identifying the relationships of climate and physiological responses of a  
739 beech forest using the Standardised Precipitation Index: A case study for Slovakia. *Journal of  
740 Hydrology and Hydromechanics* 64, 246–251.
- 741 Williams, M., Law, B. E., Anthoni, P. M., Unsworth, M. H., 2001. Use of a simulation model and

- 742 ecosystem flux data to examine carbon-water interactions in ponderosa pine. *Tree Physiology*  
743 21, 287–298.
- 744 Xenakis, G., Ash, A., Siebicke, L., Perks, M., Morison, J. I., 2021. Comparison of the carbon,  
745 water, and energy balances of mature stand and clear-fell stages in a British Sitka spruce forest  
746 and the impact of the 2018 drought. *Agricultural and Forest Meteorology* 306 (November 2020),  
747 108437.
- 748 URL <https://doi.org/10.1016/j.agrformet.2021.108437>
- 749 Yang, J., Magney, T., Yan, D., Knowles, J., Smith, W., Scott, R., Barron-Gafford, G., 2020. The  
750 Photochemical Reflectance Index (PRI) captures the ecohydrologic sensitivity of a semiarid  
751 mixed conifer forest. *Journal of Geophysical Research: Biogeosciences* 125.
- 752 Zhang, S.-B., Cao, K.-F., Fan, Z.-X., Zhang, J.-L., 8 2013. Potential hydraulic efficiency in an-  
753 giosperm trees increases with growth-site temperature but has no trade-off with mechanical  
754 strength. *Global Ecology and Biogeography* 22, 971–981.
- 755 URL <https://onlinelibrary.wiley.com/doi/10.1111/geb.12056>
- 756 Zhou, S., Zhang, Y., Williams, A. P., Gentine, P., 1 2019. Projected increases in intensity, frequency,  
757 and terrestrial carbon costs of compound drought and aridity events. *Science Advances* 5.
- 758 URL <https://www.science.org/doi/10.1126/sciadv.aau5740>
- 759 Zhu, S. D., Chen, Y. J., Ye, Q., He, P. C., Liu, H., Li, R. H., Fu, P. L., Jiang, G. F., Cao, K. F., 5 2018.  
760 Leaf turgor loss point is correlated with drought tolerance and leaf carbon economics traits. *Tree  
761 Physiology* 38, 658–663.
- 762 Zhuang, J., Yu, G. R., Nakayama, K., 2014. A series RCL circuit theory for analyzing non-steady-  
763 state water uptake of maize plants. *Scientific Reports* 4.
- 764 Zweifel, R., Zimmermann, L., Newberry, D. M., 2005. Modeling tree water deficit from microclimate:  
765 An approach to quantifying drought stress. *Tree Physiology* 25, 147–156.

Table 1: Main concepts of electrical theory and their equivalence in plant hydraulics.

Concept	Electrical [Units]	Hydraulic [Units]
Quantity	Charge [ $C$ ]	Volume [ $L$ ]
Quantity flux	Current [ $C s^{-1} = A$ ]	Volume flow rate [ $L s^{-1}$ ]
Flux density	Current density [ $C m^{-2} s^{-1} = A m^{-2}$ ]	Velocity [ $L m^{-2} s^{-1}$ ]
Potential	Electrical potential [ $J C^{-1} = V$ ]	Water potential [ $J L^{-1} = kPa$ ]
Storage	Capacitance [ $F = C V^{-1}$ ]	Water storage [ $L kPa^{-1}$ ]

Table 2: Number of days ( $N$ ) hydraulic efficiency was in the waters stress  $\eta_s$ , most efficient( $\eta_{me}$ ), moderately efficient ( $\eta_{md}$ ), moderately unrestricted ( $\eta_{mu}$ ) and unrestricted zones ( $\eta_u$ ), and the mean efficiency( $\bar{\eta}$ ) during the monitoring period. The number in parenthesis is the standard error of the mean. The number of days was calculated for individual trees and for each year of available flux data at the ecosystem level.

	$N_{\eta_s}$	$N_{\eta_{me}}$	$N_{\eta_{md}}$	$N_{\eta_{mu}}$	$N_{\eta_u}$	$\bar{\eta}$
<i>Tree level</i>						
2	15	2	6	10	49	0.78 ( $\pm 0.0051$ )
4	-	-	-	-	82	1 ( $\pm 0.0001$ )
5	-	-	-	-	81	0.99 ( $\pm 0.0003$ )
7	52	4	4	5	18	0.36 ( $\pm 0.0066$ )
8	-	-	-	1	82	0.99 ( $\pm 0.0004$ )
9	67	3	4	2	7	0.17 ( $\pm 0.0052$ )
<i>Ecosystem level</i>						
2015	13	5	11	36	301	0.91 ( $\pm 0.0014$ )
2016	21	3	7	18	315	0.91 ( $\pm 0.0019$ )
2017	24	11	15	32	283	0.88 ( $\pm 0.0019$ )
2018	115	32	38	38	143	0.63 ( $\pm 0.003$ )
2019	43	27	35	66	195	0.79 ( $\pm 0.0024$ )
2020	49	19	31	45	222	0.8 ( $\pm 0.0026$ )

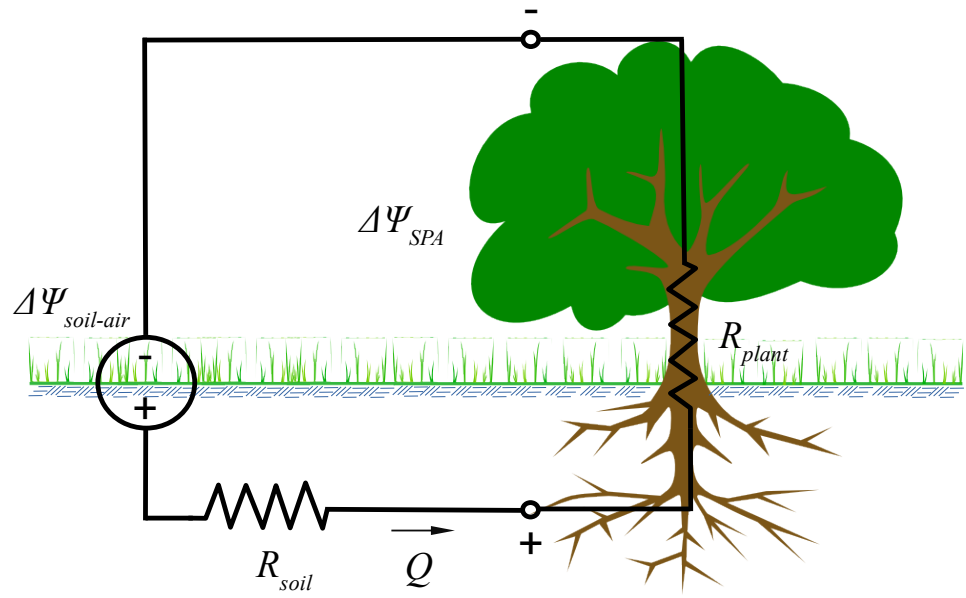


Figure 1: An electric close circuit analogy of the soil-plant-atmosphere continuum with two resistors and one source.



Figure 2: SFM1 sensor used to measure stem sap flow.

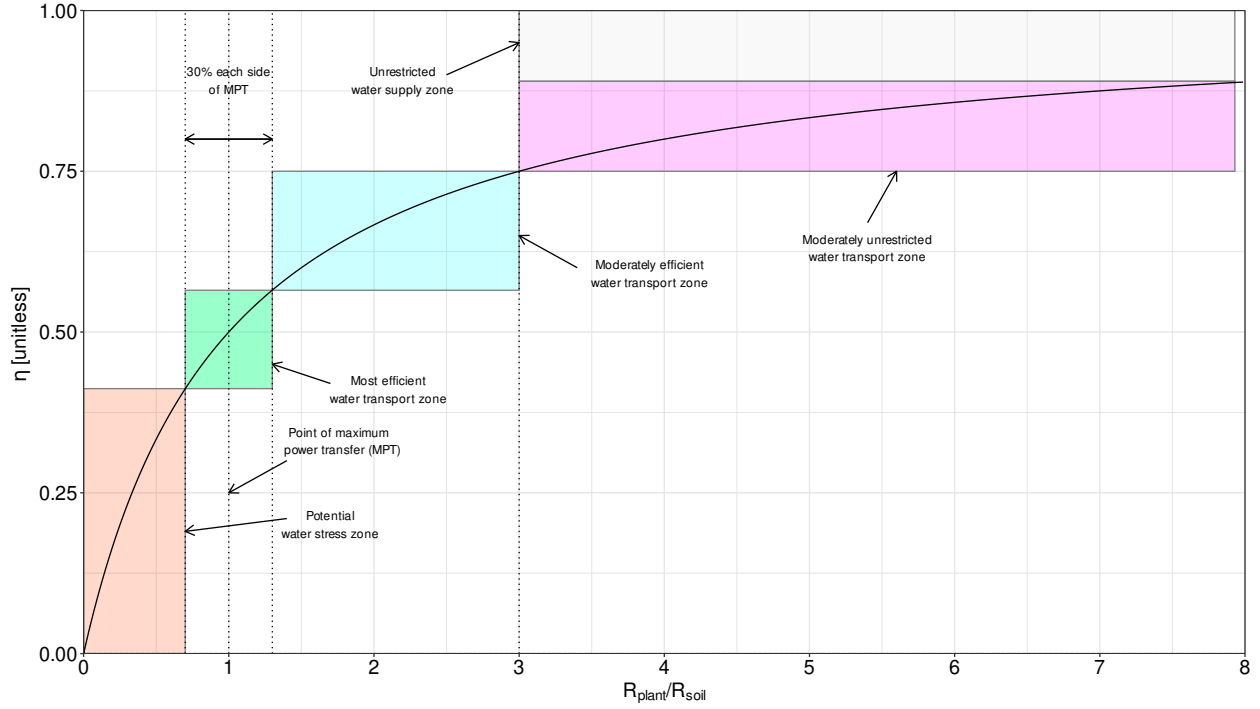


Figure 3: Response function showing the relationship between the ratio of the plant ( $R_{plant}$ ) to soil ( $R_{soil}$ ) resistance against hydraulic efficiency. The Maximum Power Transfer is defined as the point where the ratio equals one ( $R_{plant} = R_{soil}$ ). From there, five water transport zones can be defined starting from the MPT point, assuming a 30% variance around it, defining the most efficient zone ( $0.412 < \eta_{ms} \leq 0.565$ ). Other zones include potential water stress ( $0 < \eta_s \leq 0.412$ ), moderately efficient ( $0.565 < \eta_{md} \leq 0.75$ ), moderately unrestricted ( $0.75 < \eta_{mu} \leq 0.89$ ), and unrestricted water transport ( $0.89 < \eta_u \leq 1$ ). Each zone is colour-coded, and the same scheme is used throughout the illustrations.

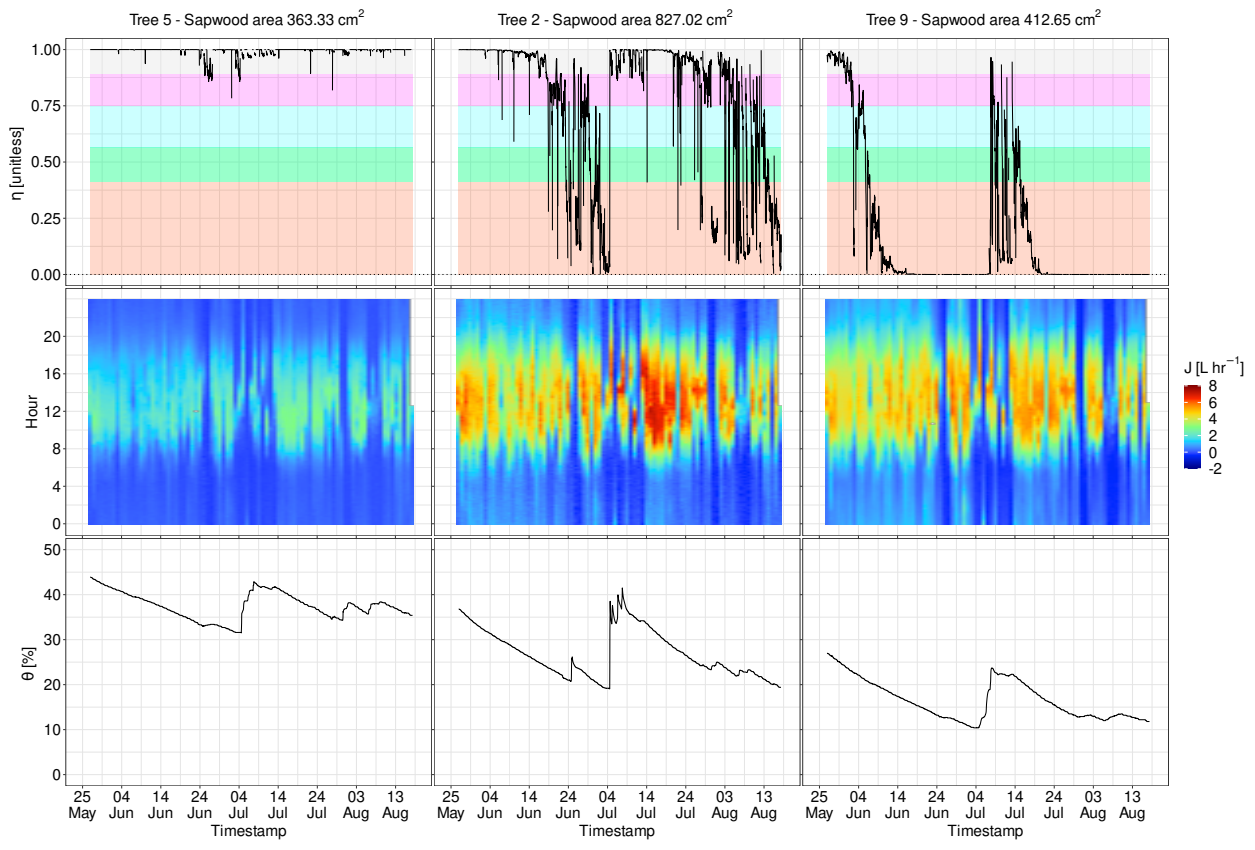


Figure 4: Hydraulic efficiency (top,  $\eta$  unitless), sap flow (middle,  $J$ ,  $L \cdot hr^{-1}$ ) and volumetric water content (bottom,  $\theta$ , %) for three trees with different levels of soil water and water stress. Colour bands in the top three panels correspond to the colour-coded zones shown in Figure 3.

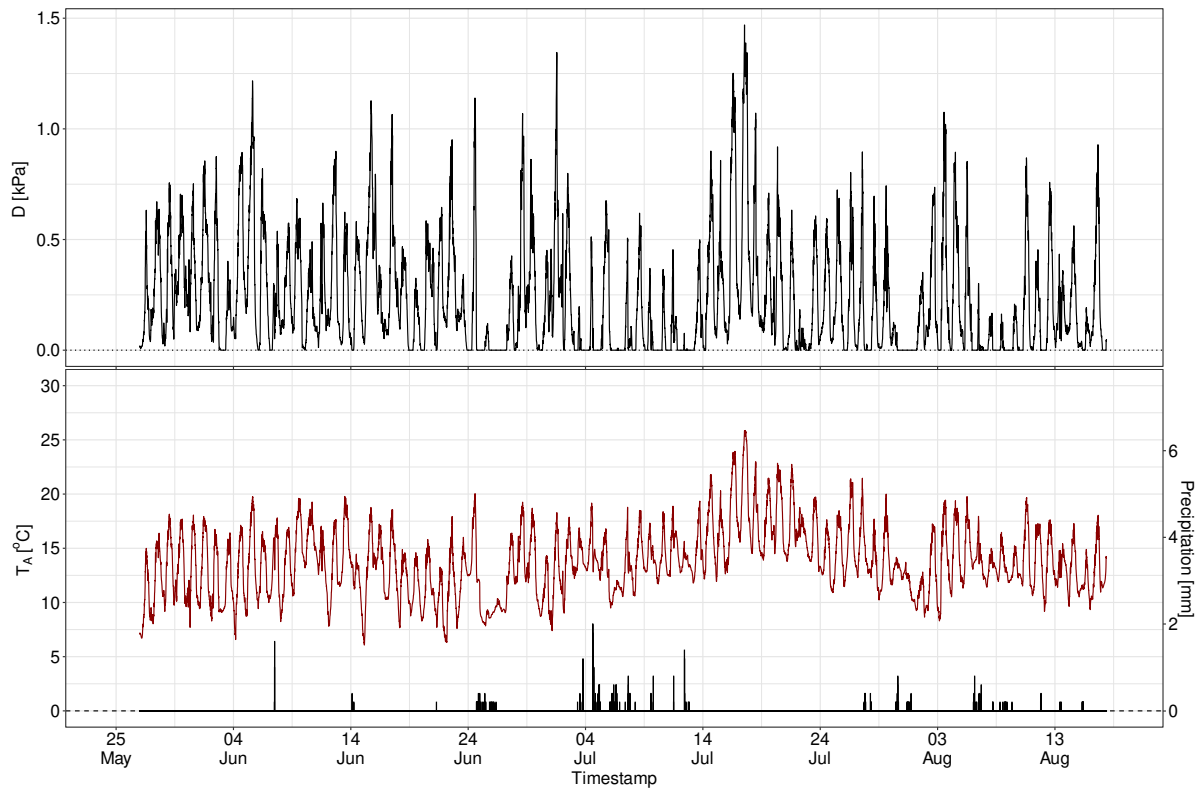


Figure 5: Timeseries of 10-min vapour pressure deficit ( $D$ , kPa), air temperature ( $T_A$ , °C) and total precipitation ( $Pr$ , mm) during the period of sap flow measurements between May and August at Harwood Forest, Northumberland. All variables were measured over the forest canopy at 32 m above the ground.

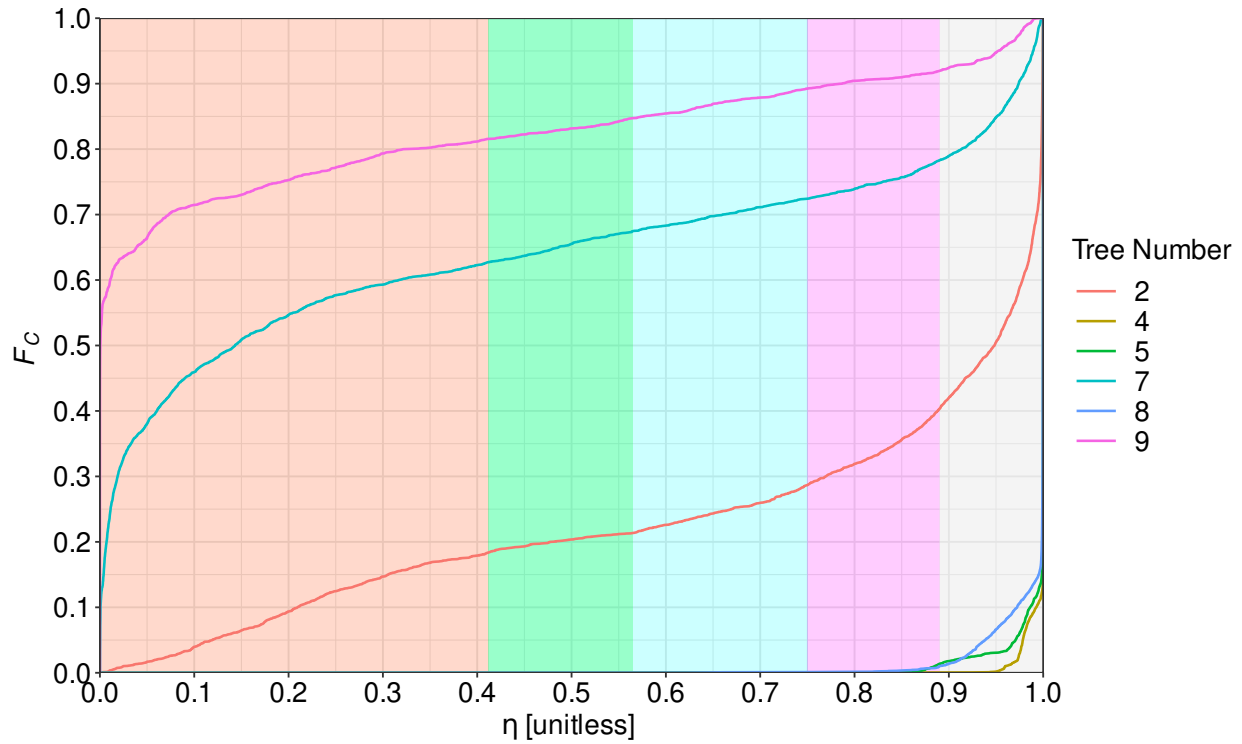


Figure 6: Empirical cumulative density functions ( $F_C$ ) of hydraulic efficiency ( $\eta$ ) plotted against efficiency for the six trees with complete timeseries over the monitoring period. Colour bands correspond to the five efficiency zones.

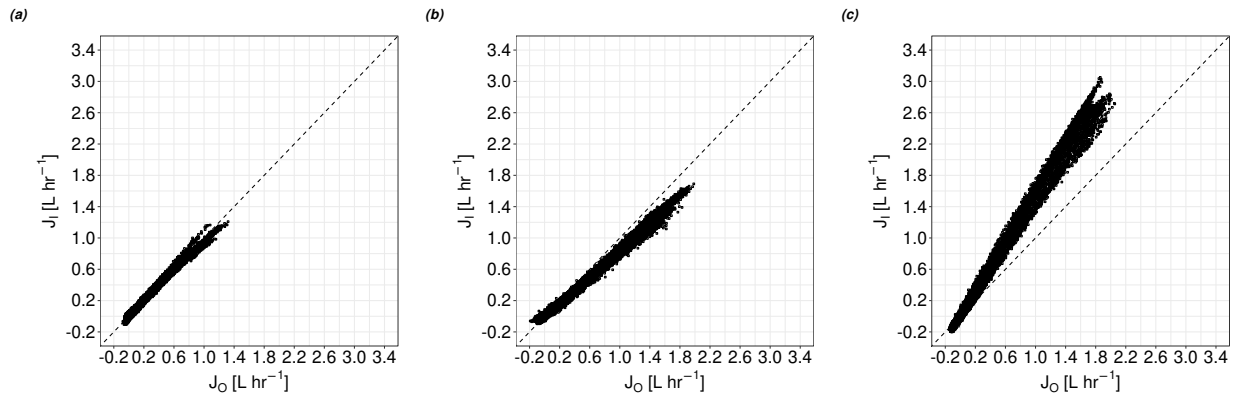


Figure 7: Sap flow of the inner measurement points of the sensor ( $J_I$ , L m<sup>-1</sup>) versus the outer measurement ( $J_O$ , L m<sup>-1</sup>) during the full measurement period for (a) tree 5, (b) tree 2, and (c) tree 9. Deviation from the 1:1 line shows radial variability of water movement within the xylem.

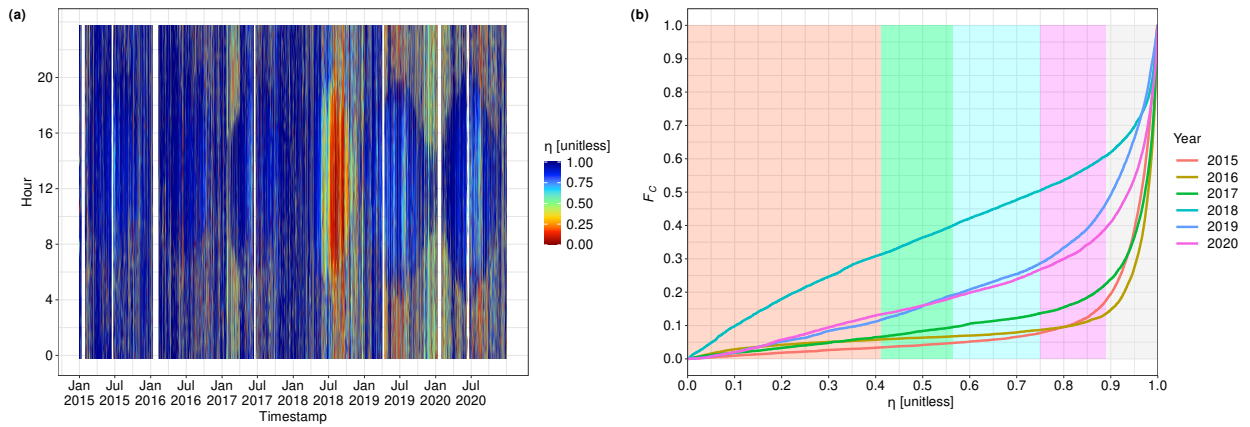


Figure 8: Fingerprint plot (a) and empirical cumulative density functions (b) for stand level hydraulic efficiency calculated from evapotranspiration measurements from the eddy covariance tower at Harwood Forest, Northumberland. The colour bands in panel (b) correspond to the hydraulic efficiency zones.

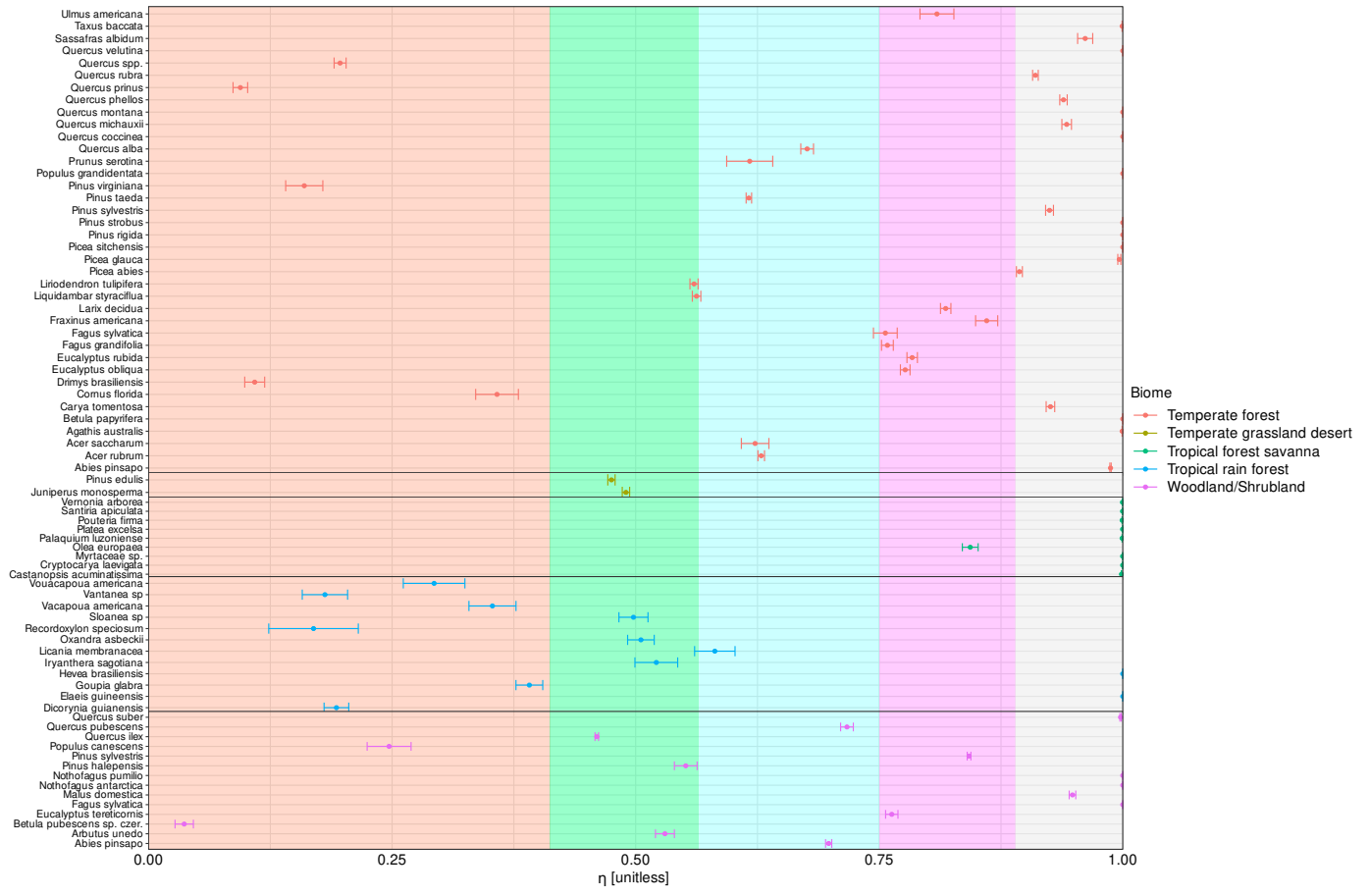


Figure 9: Mean hydraulic efficiency of 75 species across 71 sites and five biomes based on the SAPFLUXNET classification. Error bars show the standard error of the mean. Coloured points show different biomes. Colour bands correspond to the five hydraulic efficiency zones shown in Figure 3.